Stars In The Infrared : Results From IRAS

HENNY J.G.L.M. LAMERS[1,2] and LAURENS B.F.M. WATERS[3]

[1] Astronomical Institute at Utrecht
[2] SRON Laboratory for Space Research in Utrecht
[3] SRON Laboratory for Space Research in Groningen

1 INTRODUCTION

The Infrared Astronomical Satellite (IRAS) was the first instrument to observe a large number of stars in the wavelength range between 12 and 100 micron. Since the satellite was designed to scan the entire sky the observations are unbiased: every object brighter than the limiting magnitudes of the instruments was detected. This led to the observations of a very large number of known sources (Planets, Stars, Circumstellar and Interstellar Clouds and Galaxies) but also to the discovery of several new types of objects such as the dust-rings around Vega-type stars, the Interstellar Cirrus and the IR-galaxies.

The results of IRAS have been published in a large number of papers and in the proceedings of several conferences devoted partly or entirely to IRAS. The most important ones are: "Light on Dark Matter" (Israel et al., 1986); "Starformation in Galaxies" (Lonsdale-Persson, 1987); "From Comets to Cosmology" (Lawrence, 1988).

In this paper we will review the results of the stellar observations by IRAS. Before the launch of IRAS the main stellar results were expected in the field of star-formation and of cool stars. However IRAS has also contributed enormously to the studies of hot stars because IRAS detected the free-free radiation from many hot stars with gaseous envelopes or rings and the thermal radiation from many hot stars with circumstellar dust. Considering the very large number of papers published about the stellar observations of IRAS we have to be selective in this review. This selection is unavoidably biased by our own interest. So, instead of presenting a kaleidoscope of the many IRAS results, we will present the results in a more or less coherent way, in which the stellar evolution serves as a guideline. The theory of the IR free-free emission will be discussed in the context of the hot stars and the theory of dust-emission will be discussd in the context of the cool stars. The studies of the dust-rings around Vega-type stars will not be discussed here, because they are described elsewhere in this volume.

The IRAS mission will be described in Section 2. The IRAS results of early type

stars are discussed in Sections 3 and 4. The IRAS results of late type stars are reviewed in Section 5.

2 IRAS

2.1 The IRAS Mission

The IRAS satellite operated between January 1983 and November 1983 during ten months. This was just short of the planned twelve months of operation which were necessary to make two scans of the whole sky. The mission and its instruments are described in the Explanatory Supplement to the IRAS Point- Source Catalogue (Beichman et al. 1988).

The instrument consisted of a 60 cm Ritchey-Chretien telescope which was cooled by liquid Helium to a temperature of 2 - 5 K. The satellite was in a low-earth near-polar orbit with an orbital precession of 1 degree per day with the telescope pointing away from the earth. This combination of orbit and attitude allowed the instrument to scan the celestial sphere in 6 months. The focal plane consisted of a wide band photometric system, with four bands centered at 12, 25, 60 and 100 μm. The transmission function of the IRAS filters is shown in Fig. 1. The limiting fluxes of the photometers for point-sources were 0.5, 0.5, 0.5 and 1.5 Jansky respectively (1 Jansky = 10^{-23} ergs/cm^{2}s Hz). The angular resolution of the photometer varied from 0.5 arcmin at 12 μm to 2 arcmin at 100 μm. In addition to this main photometric system there was also a special instrument (CPC = Chopped Photometric Channel) with a higher spatial resolution of 1.3 to 1.7 arcmin, at 50 and 100 μm, which could be used for raster scans of small selected areas.

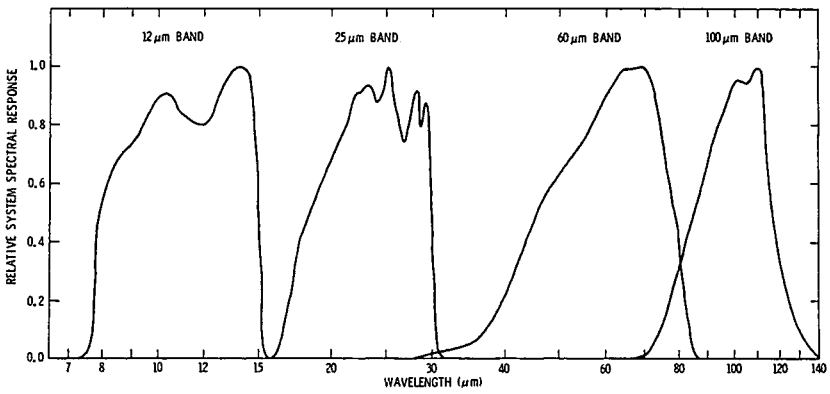

Fig. 1 The spectral response curves of the four photometric bands (from Beichman et al., 1988).

The focal instruments also contained a low-resolution spectrometer (LRS) operating

between 8 and 22 μm with a spectral resolution of $\lambda/\Delta\lambda = 20$ to 60 and a limiting flux of 10 Jy at 12 and 25 μm.

During the IRAS mission 96 percent of the sky was observed resulting in the observations of

250 000	point sources
20 000	extended sources
5 000	LRS spectra

One of the most important factors for the success of IRAS was the fast publication of the data in the IRAS Point Source Catalogue (JISWG, 1988); the IRAS Serendipitous Survey Catalogue (Kleinmann, 1986); The IRAS Faint Source Survey (Moshie, 1989) and the Atlas of IRAS Low Resolution Spectra (IRAS Science Team, 1986). All IRAS data bases are interactively available via the Geisha System at the SRON Laboratory for Space Research in Groningen and at IPAC in Pasadena.

2.2 IRAS photometry of stars

The IRAS magnitudes of the stars published in the PSC have to be colour-corrected in order to reduce them to the absolutely calibrated mono-chromatic fluxes at 12, 25, 60 and 100 μm. This colour-correction is described in the IRAS Explanatory Supplement. The zero points of the colour-corrected IRAS magnitudes are defined by the flux from a black-body of T = 10 000 K with an angular diameter of 1.41 10^{-8} radians. This implies the following fluxes for the IRAS magnitudes:

[12] = 0.00 :	2.83 10^{-22}	erg/cm^2 s Hz at 12 μm
[25] = 0.00 :	6.73 10^{-23}	erg/cm^2 s Hz at 25 μm
[60] = 0.00 :	1.19 10^{-23}	erg/cm^2 s Hz at 60 μm
[100] = 0.00 :	0.43 10^{-23}	erg/cm^2 s Hz at 100 μm

With these definitions Vega has a magnitude of [12] = -0.02.

The IRAS observations of stars in the Bright Star Catalogue (Hoffleit and Jaschek, 1982) studied by Waters et al. (1987a) are shown in Figure 2. This figure shows the colour-colour plots of V-[12], V-[25], V-[60] and V-[100] versus B-V. Fig 2 shows that the majority of the stars fall in a narrow and well-defined band. This band corresponds approximately to the colour-colour relation of black- bodies and it consists of normal stars without IR excess. The band is narrow because the interstellar reddening displaces a star from its intrinsic position in a direction almost parallel to the band. This fortunate circumstance implies that stars which deviate from the band have abnormal colours: the stars with an IR excess are located above the band. Therefore the four colour plots presented in Fig. 2 provide a very efficient way to detect stars with excess fluxes in the IRAS bands, at least for stars with B-V $\lesssim$ 1.3.

The band is most easily seen in Figs. 2A and 2B. In Fig. 2C the band is only sparsely populated at B-V $\lesssim$ 1.0, but it can still be detected as the lower limit in

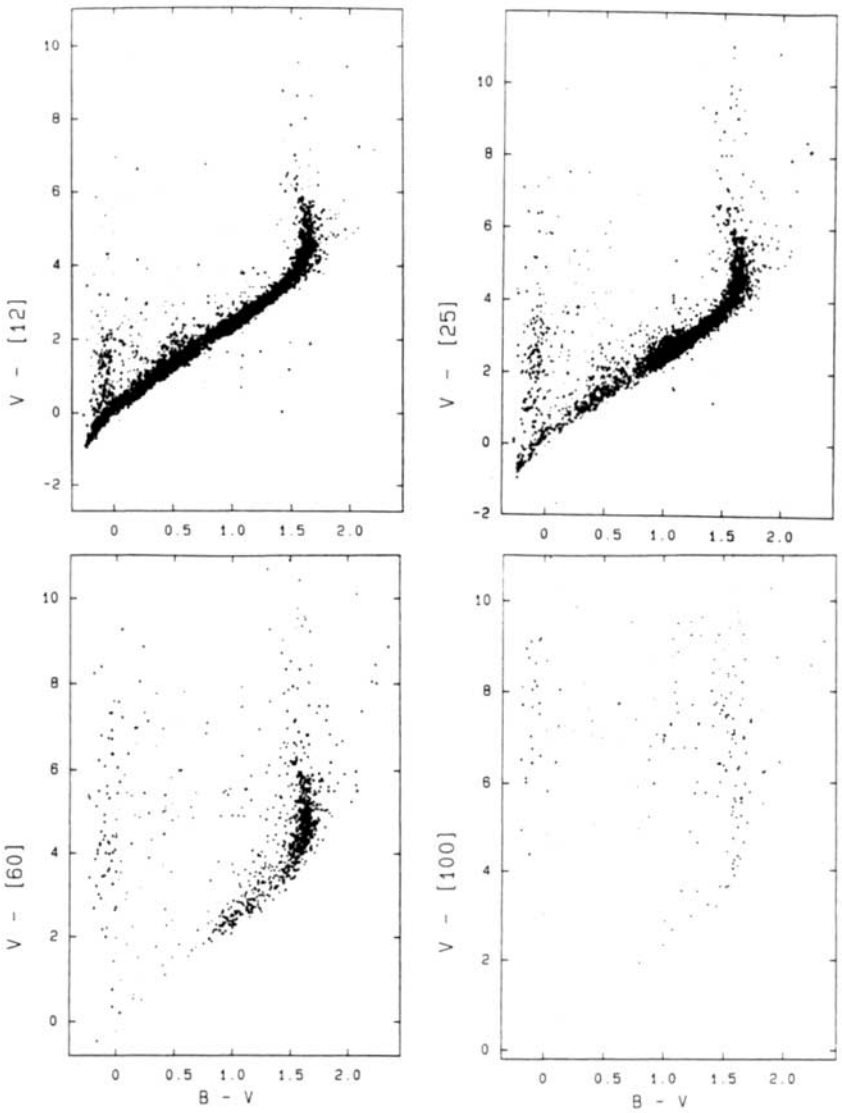

Fig. 2 Colour-colour diagrams of all stars in the Bright Star Catalogue observed with IRAS. Notice the narrow band of stars without excess. This narrow band is sparsely populated in V-[60] and V-[100] because the flux of normal stars at long wavelengths is very small. The stars near B-V $\simeq$ 0.0 with excess are mostly Be-stars (from Waters et al. 1987a).

the range of 0 $\lesssim$ B-V $\lesssim$ 1.0. This is obviously due to the fact that the flux of early type stars at 60 μm is so low that only the brightest early type stars are above the IRAS detction limit. The stars with IR excess at 60 μm (i.e. those 1 magn or more

above the lower limit) are more easily observed by IRAS. Therefore the apparent ratio of early type stars with excess and without excess seems to increase towards longer wavelengths due to the observational selection effect.

The band turns upwards near B-V $\simeq$ 1.5. This is the location of the late type stars of types later than K 3. The larger scatter in the IRAS colour-colour plots for B-V $\gtrsim$ 1.5 is due to scatter in the intrinsic relations and to the effect of interstellar reddening. The intrinsic colour-colour relations of the stars of types B2 to K3 of class IV-V and F0 to M5 of class II-III have been determined from the data presented in Figure 2 and are compared with the predictions for O, B, A stars from Kurucz's (1979) blanketed LTE models by Waters et al. (1987a). They found that the stars are about 0.1 magn brighter at 12 and 25 μm than predicted by the models.

Fig. 2 shows that a considerable number of early type stars with B-V $\lesssim$ 0.2 has an IR excess at all IRAS bands. These are mainly the Be-stars with IR excess from the circumstellar disks.

2.3 IRAS-LRS spectra of stars

A sample of LRS spectra is shown in Fig. 3 (from IRAS Explan. Suppl). The normal star shows a black-body like energy distribution. One of the most important characteristics of the LRS spectra is the fact that they easily distinguish between stars with O-rich dust and C-rich dust. O-rich dust has silicate features at 9.7 and 18 μm and C-rich dust has a feature at 11.2 μm. These features are in emission when the circumstellar dust is optically thin at their wavelengths and in absorption when the CS dust is optically thick. Fig. 3 shows examples of stars with C-rich and O-rich dust. Fig. 3 also shows examples of gaseous emission line spectra of planetary nebulae.

3 FREE-FREE AND FREE-BOUND RADIATION FROM EARLY TYPE STARS

3.1 Free-free and free-bound emission from stellar winds

Early type stars with mass loss are surrounded by ionized circumstellar gas. This ionized gas can produce an IR excess due to free-free (ff) and free-bound (fb) emission. The theory of IR ff and fb emission from stellar winds was first developed by Barlow and Cohen (1977) and by Cassinelli and Hartmann (1977). It was improved and extended by Lamers and Waters (1984a) and Waters and Lamers (1984) who introduced the concept of the IR curve-of-growth analysis for an easy diagnostic of the IR excess from stellar winds. Lamers and Waters (1984b) also studied the effects of clumping and of the presence of a corona on the IR excess. Here we will briefly review the theory of the IR excess from stellar winds.

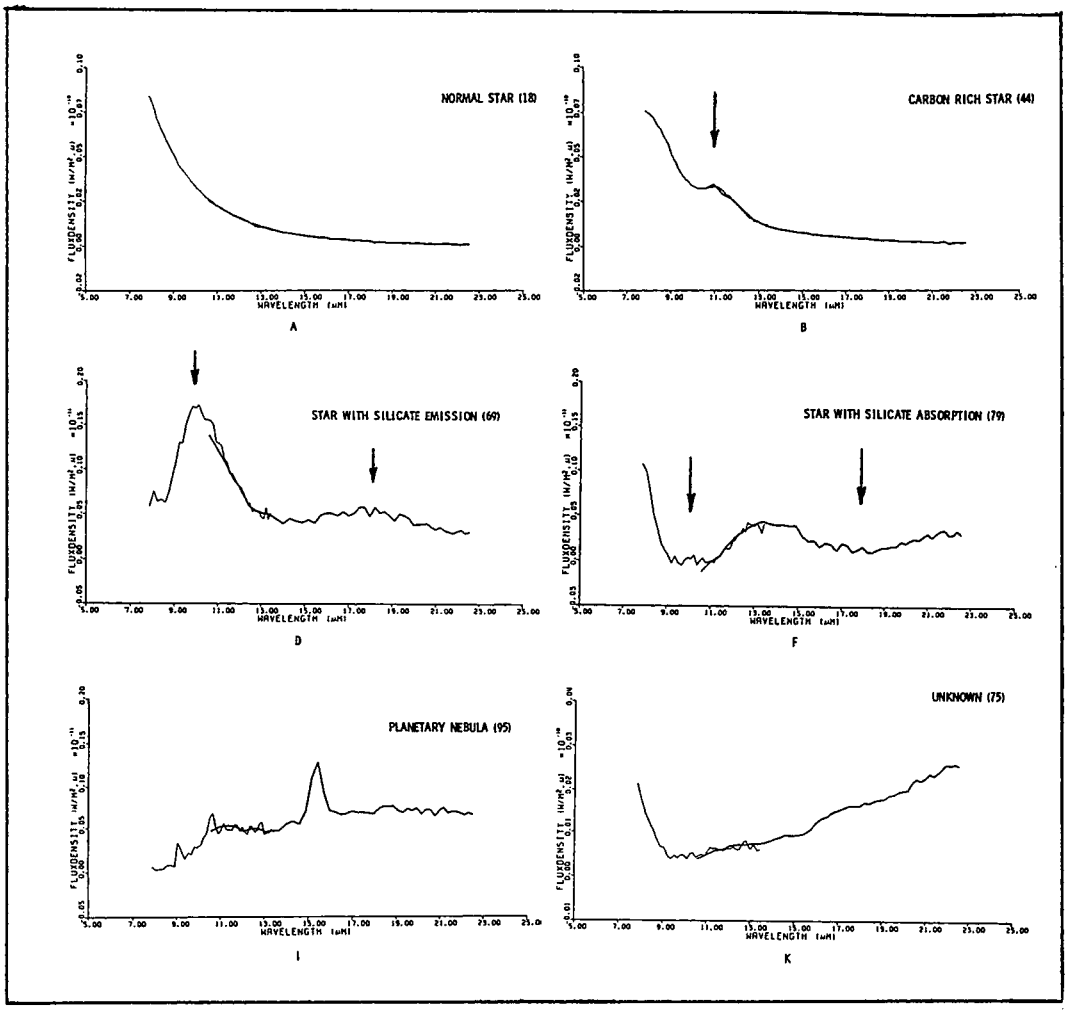

Fig. 3 IRAS LRS spectra in the wavelength range of 9 to 22 μ of some representative stars (from Beichman et al., 1988).

The opacity of ff and fb processes at frequencies $h\nu \ll kT$ is

$$\kappa_\nu = 3.69\ 10^8 (h/k) Z^2 (g + b) T^{-3/2} \nu^{-2} \gamma n_i^2 \qquad (1)$$

in cm^{-1}, where ν is the frequency in Hz, T is the temperature, Z^2 is the mean value of the squared atomic charge, g and b are the gaunt-factors for ff and fb emission, γ is the ratio between the electron and ion density by number and n_i is the ion-density in cm^{-3}. The ion-density is related to the mass loss rate via the mass continuity equation

$$n_i(r) = \dot{M} / 4\pi\, r^2\, v(r) \mu m_H \qquad (2)$$

where μm_H is the mean atomic weight of the ions. Notice that the opacity is proportional to $n_i^2 \sim \dot{M}^2$ and to λ^2. So the effective radius, defined as $r(\tau_\lambda = 1/3)$, of a star with a wind increases to longer wavelengths.

In a very crude approximation we can estimate that the flux from a star+wind is proportional to $r^2(\tau_\lambda = 1/3)\, B_\nu$. So if the effective radius of the star+wind becomes larger than R_* in the IR and if the temperature of the wind is not much smaller than that of photosphere, the flux in the infrared will be larger than from the photosphere alone by a factor

$$\mathrm{F(star + wind)/F(photosphere)} \simeq r^2(\tau_\lambda = 1/3)\, B_\nu\{r(\tau_\lambda = 1/3)\}/R_*^2\, B_\nu\,(\mathrm{T_{eff}}) \quad (3)$$

This equation shows that for a star with an isothermal wind at T(wind) $\simeq$ $\mathrm{T_{eff}}$ the excess will be significant only at wavelengths where $r(\tau_\lambda = 1/3) > R_*$. It also shows that if the wind is much cooler than the photosphere, the IR flux from a star with mass loss might be actually *smaller* than that of the photosphere. In this case the star will have an IR deficiency because the ff absorption in the wind is more important than the ff emission. Equ. 3 can also be used to explain the wavelength-dependence of the IR excess. Since the wavelength-dependence of the IR excess depends on the wavelength dependence of the effective radius, which in turn depends on the radial density distribution of the wind, the IR excess as a function of wavelength can be used to derive the density distribution and hence the mass loss and/or the velocity distribution in the wind.

For isothermal winds the IR excess can be analysed by means of the curve of growth method, which is based on accurate numerical solutions of the radiative transfer equation for ff and fb processes (Lamers and Waters, 1984a). For a given velocity-law of the stellar wind the IR excess depends on a simple quantity $E(r)$ which is the product of the wavelength-dependent function $\lambda^2(g + b)$ and a constant X_* which involves the stellar radius, the mass loss rate, the terminal velocity and the temperature of the wind.

$$E(\lambda) = \lambda^2(g + b)X_* \quad (4a)$$

$$X_* = 5.34\, 10^{31} Z^2 \gamma\, \dot{M}^2\, T^{-3/2} \mu^{-2} v_\infty^{-2} R_*^{-3} \quad (4b)$$

The parameter $E(\lambda)$ is a measure of the radial optical depth of the wind to ff and bf opacity. The relation between the excess and $E(\lambda)$ is called the curve of growth. Waters and Lamers (1984) have published curves of growth for various velocity laws and gaunt factors. The observational curve of growth i.e. the IR excess in magn as a function of $\log\{\lambda^2(g + b)\}$ can be compared with theoretical curves of growth for various velocity laws. The comparison between the observed and predicted curves of growth gives the velocity law of the wind, and the horizontal displacement of the observed curve with respect to the theoretical curve gives the value of the constant X_* from which the mass loss rate can be derived if the other quantities are known.

Table 1 gives the expected IR excess of a typical O-star calculated by means of the curves of growth. The velocity law in the wind is assumed to be of the type

$$v(r) = v_\infty\{0.01 + 0.99(1 - r/R_*)^\beta\} \quad (5)$$

with $v_\infty = 2000$ km/s and $\beta = 1$. The table shows that an IR excess larger than 0.1 magn can be expected at $\lambda \geq 50\mu$ if $\dot{M} = 1\ 10^{-6} M_\odot$/yr; at $\lambda \geq 10\mu$ if $\dot{M} = 1\ 10^{-5} M_\odot$/yr and at $\lambda \geq 1\mu$ if $\dot{M} = 1\ 10^{-4} M_\odot$/yr. The data in this table show that a significant IR excess at the IRAS wavelengths of 12 and 25 μm due to ff and fb emission from the winds of O-stars can only be expected for stars with mass loss rates larger than $10^{-5} M_\odot$/yr. Since the mass loss rate of O stars is a strong function of the stellar luminosity (Garmany and Conti, 1984) the excess will only be observable at $\lambda \geq 10\mu$ in O stars with $L \geq 2\ 10^6 L_\odot$.

Table 1. The free-free and free-bound excess of a typical O-star

	Δm_ν (magn)					
λ	$\dot{M} = 1\ 10^{-6}$	$3\ 10^{-6}$	$1\ 10^{-5}$	$3\ 10^{-5}$	$1\ 10^{-4}$	$M_\odot$/yr
1μ	0.00	0.00	0.00	0.02	0.11	
3μ	0.00	0.00	0.02	0.08	0.61	
10μ	0.00	0.02	0.13	0.70	1.80	
30μ	0.03	0.14	0.76	1.88	3.25	
100μ	0.20	0.92	2.08	3.50	5.23	
300μ	0.92	2.05	3.52	5.27	6.94	
1mm	2.24	3.78	5.45	7.12	8.78	
3mm	3.81	5.48	7.14	8.81	10.48	
1cm	5.62	7.31	8.97	10.64	12.30	
3cm	7.28	8.97	10.62	12.28	13.95	
10cm	9.14	10.82	12.47	14.14	15.80	

Parameters: $T_{eff} = 40000\ K$, $T_W = 32000\ K$, $R_* = 30 R_\odot$, $v_\infty = 2000$ km/s, $v_0 = 20$ km/s, $\beta = 1.0$.

Table 1 shows that the excess in magnitudes is larger at 60 and 100 μm. However at such long wavelengths the O stars are so faint that even with the excess most O stars were not detectable by IRAS except for a few of the brightest ones.

Fig. 4 shows an example of the observed IR excess of an O-star. The visual and IR energy distribution of the star ζ Pup is compared with that predicted from the photosphere and from the star with a radiation driven wind. The observed energy distribution agrees very well with the predictions for a mass loss rate of $6\ 10^{-6} M_\odot$/yr.

The IR energy distribution of P Cygni ws studied by Waters and Wesselius (1986) and by Pauldrach and Puls (1990) who both conclude that the velocity law is

much slower than for normal supergiants. In normal OB supergiants the velocity of $v = 0.5v_\infty$ is reached at $r \simeq 2R_*$, whereas the wind of P Cygni reaches $v = 0.5v = 110$ km/s at $5R_*$. These studies show the possibility of deriving the density distribution of stellar winds from IR observations, provided that these observations have sufficient accuracy.

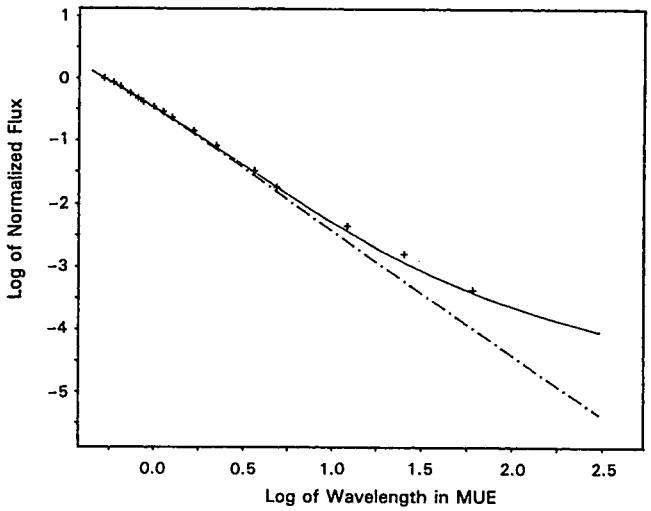

Fig. 4 The observed energy distribution of the star ζ Pup (O4If) as an example of the free-free and free-bound IR excess due to a stellar wind. The dashed line is the predicted spectrum of an O-star without a wind. The full line is the predicted spectrum of an O-star with a radiation driven wind with a mass loss rate of $6\ 10^{-6} M_\odot/yr$ *(from Kudritzki et al., 1988).*

3.2 The IR excess from disks of Be stars

The IRAS data in Fig. 2 show that many Be stars have an IR excess of several magnitudes at 12, 25 and 60 μm. The optical emission lines of the Be stars indicate that the stars are surrounded by a rotating gaseous envelope. The line profiles together with the optical polarization clearly indicate that this rotating envelope is in the form of an equatorial disk with a typical density of 10^9 to $10^{11}\mathrm{cm}^{-3}$.

The IRAS fluxes of > 100 Be stars have been studied in detail by Waters (1986), Coté and Waters (1987) and Waters et al. (1987). Fig. 5A shows the energy distribution of two typical Be stars: δ Cen and χ Oph. These distributions show an excess at $\lambda > 3\mu$m relative to the flux predicted by model photospheres. The shape of the excess is typical for ff and fb emission. The IR excess can be interpreted by a simple model consisting of a star with a disk with a constant opening angle of

about 30 to 60 degrees (in agreement with the information from the polarization) and a density distribution of

$$\rho = \rho_0 (r/R_*)^{-n} \tag{6}$$

The predicted curve of growth for such a simple model is shown in Fig. 6. It consists of three nearly linear parts. 1. At small λ where the whole disk is optically thin to ff and bf opacity the excess in $2.5\Delta m_\lambda$ is proportional to the emission measure and hence to $\lambda^2(g+b)$. 2. At λ larger than some critical value (usually between 3 and 10 μm) the inner part of the disk is optically thick and the outer part is optically thin. In this regime the slope of the curve of growth is $2/(2n-1)$ where n is the exponent of the density distribution (eq. 6). The critical wavelength where the two linear parts meet depends on ρ_0. 3. If the disk has a finite size, i.e. it is truncated at some distance R_d from the star, the curve of growth will be flat and the excess will be constant at long wavelengths where the whole disk is optically thick. The turnover between this horizontal part and the $2/(2n-1)$ part depends on the value of R_d.

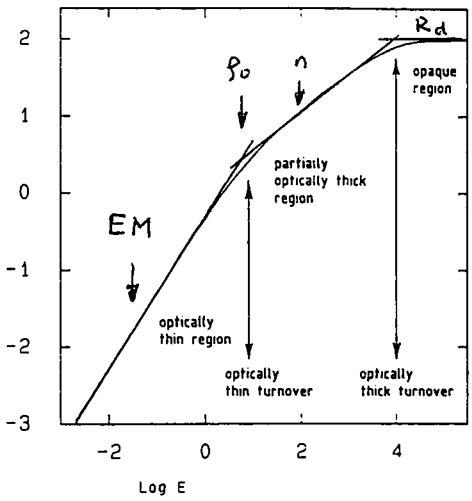

Fig. 6 The predicted curve of growth for the IR excess by ff and fb emission from a disk with a density distribution $\rho(r) = \rho_0(r/R_*)^{-n}$. The three nearly linear parts are indicated together with the parameter that can be derived from the various parts (from Waters, 1986).

The observed curves of growth of Be stars agree very well with these predictions (Fig. 5B): they can be fitted with two linear parts. One of these is the optically thin part with a slope of 1 which immediately gives en estimate of the emission measure of the disk. The slope of the second part gives the value of n and the turnover gives the value of ρ_0. The empirical curve of growth does not show the horizontal part which means that the disks of these two stars extend to beyond $10R_*$. Using the